CrossMark

Fluorescence vesicles by self-assembly of oligo(biphenylene vinylene) bolaamphiphiles in *n*-hexane

In-Wook Hwang [a,*], Yong-Rok Kim [b,*]

[a] Advanced Photonics Research Institute, Gwangju Institute of Science and Technology, Gwangju 500-712, South Korea
[b] Department of Chemistry, Yonsei University, Seoul 120-749, South Korea

ARTICLE INFO

ABSTRACT

Self-assembly of an oligo(biphenylene vinylene); OBPV bolaamphiphile with two polar coils of significantly long poly(propylene oxide); PPO ($n = 21$) at each end generated a fluorescent vesicle in apolar *n*-hexane. The vesicle efficiently produced *trans*-stilbene-like OBPV excimer emissions, as evidenced by an intense, redshifted, structured fluorescence spectrum with a long decay time of 5.0 ± 0.1 ns. An OBPV chromophore bound at both sides via a polar coil-to-coil interaction in apolar *n*-hexane was conducive to OBPV excimer emission, as evident from analysis of the spectroscopic data obtained from OBPVs with different PPO coil lengths ($n = 13, 21, 34$).

Crown Copyright © 2013 Published by Elsevier B.V. All rights reserved.

1. Introduction

Bolaamphiphilic (BA) molecules, which contain a hydrophobic skeleton with two hydrophilic moieties at each end, self-assemble into highly organized aggregates that exhibit various nanostructures, such as spherical vesicles, lamellar crystals, nanowells, and nanofibers [1]. Specific interactions such as charge-transfer reactions [2], hydrogen bonding [3,4], and hydrophobic interactions [5] are important factors that govern the physical properties of these aggregates. However, the aggregated species frequently encountered during studies generate many questions with regard to their formation as well as their properties relative to the molecularly dissolved species. Linear spectroscopic methods, such as steady-state and time-resolved fluorescence spectroscopies, may provide detailed information on the intermolecular interactions of specific aggregates, as will be shown here.

In this study, we report a novel vesicle that was formed in apolar solution by the self-assembly of a BA material comprising an oligo(biphenylene vinylene) (OBPV) terminated at each end by a significantly long poly(propylene oxide) (PPO) coil ($n = 21$, where *n* represents the number of repeating units); this material was designated OBPV-21. Interestingly, the vesicle produced an intense, redshifted, structured fluorescence spectrum, characterized by a time-decay constant of 5.0 ± 0.1 ns. The spectrum was attributed to relaxation from the excited states of *trans*-stilbene-like OBPV excimers. Also, in apolar *n*-hexane solution, a polar coil-to-coil interaction between the long flexible PPO coils, rather than a conventional hydrophobic rod-to-rod interaction, efficiently actuated

vesicle formation and the subsequent intense excimer emission. This mode of interaction was evident from a comparative analysis of spectroscopic data obtained from OBPVs with different PPO coil lengths ($n = 13, 21, 34$).

Several previously reported triblock BA vesicles [6–8] showed excimer emissions via a hydrophobic interaction in polar or aqueous media. However, vesicles arising from the self-assembly of diblock rod-coil molecules [9,10] rarely exhibited excimer emissions, principally because of curvature [8] between the spherically organized chromophores. In this report, we demonstrate the underlying molecular interaction dynamics for the intense excimer emissions of OBPV vesicles: specifically, an OBPV chromophore bound at both ends via a polar coil-to-coil interaction produces intense excimer emission. A fluorescent vesicle that exhibited spectra that distinguished between folded and unfolded states would be of significant importance in bio-imaging and sensing applications.

The previously synthesized OBPVs were shown to form interesting liquid crystal assemblies (2D lamellar, 2D hexagonal columnar, and 3D tetragonal hockey puck) [11]; however, no further details on supramolecular self-assembly in solution were reported. Note that OBPV-21 contains a long hydrophobic π-conjugated rod (three biphenyls linked by two vinylene units) and two significantly long polar PPO coils ($n = 21$) at each end, whose longer molecular units are appropriate for self-assembly (Figure 1A).

2. Experimental

The synthesis of the OBPVs was reported previously [11]. The steady-state spectra were recorded using a Hitachi F-4500 fluorescence spectrophotometer at room temperature. A front-face alignment using a short (0.1 cm) path length fluorescence cell was

* Corresponding authors. Fax: +82 62 715 3419.
E-mail addresses: hwangiw@gist.ac.kr (I.-W. Hwang), yrkim@yonsei.ac.kr (Y.-R. Kim).
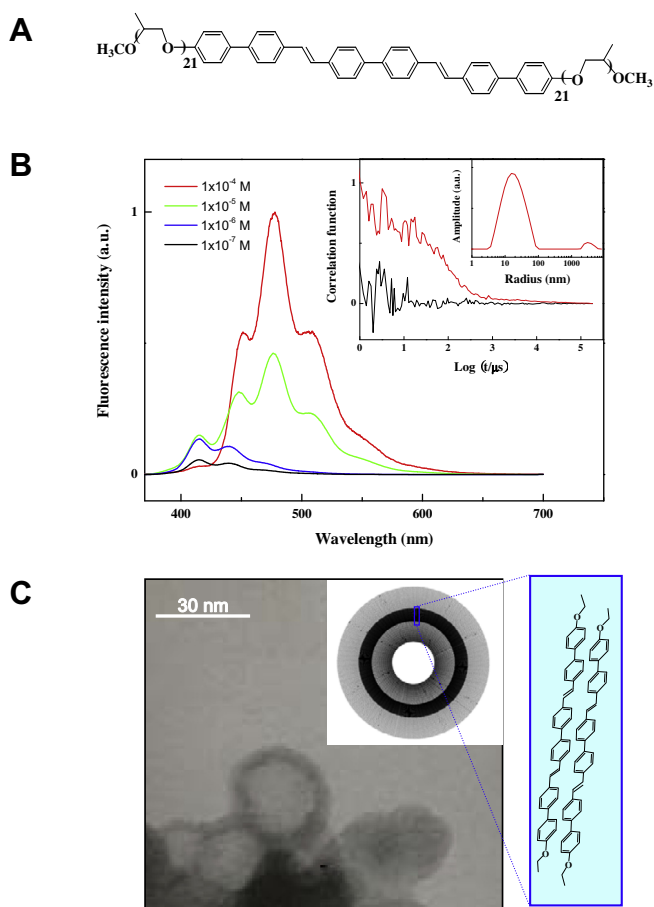
A

B

C

Figure 1. (A) Molecular structure of OBPV-21. (B) Fluorescence spectra for OBPV-21 as a function of concentration (1×10^{-7} to 1×10^{-4} M) in *n*-hexane. The insets show the DLS autocorrelation traces for the 1×10^{-7} M (black) and 1×10^{-4} M (red) solutions, and the size distribution function from the DLS data at 1×10^{-4} M. The excitation wavelength for the fluorescence spectra was 300 nm. (C) TEM image obtained after solvent removal from the 1×10^{-4} M solution; insets show a cross-section of the proposed OBPV vesicle and the molecular organization for H-aggregated OBPVs. (For interpretation of the references to colour in this figure legend, the reader is referred to the web version of this article.)

employed, particularly to avoid experimental artifacts such as self-absorption and the inner filter effect for the concentrated solutions [12]. The time-resolved fluorescence decays were measured using a time-correlated single photon counting (TCSPC) system comprising a cavity-dumped dual-jet dye laser (700 series, Coherent) pumped with a picosecond Nd–YAG laser (Antares 76-YAG, Coherent) [13]. The fluorescence-decay time constants were obtained by first deconvoluting the measured signal from the pump time profile (characterized by a full width at half maximum of ~50 ps) and then fitting to a sum of exponential terms [14]. The chi-square (χ^2) values for the fittings were 1.0–1.4. Dynamic light scattering measurements were performed using a He–Ne laser (30 mW at 632.8 nm). The detector optics employed optical fibers coupled to an ALV/SO–SIPD/DUAL detection unit, which used an EPI PM-28B power supply and ALV/PM–PD preamplifier/discriminator. The scattered light intensity was detected at a scattering angle of 60°. The signal analyzer was an ALV-5000/E/WIN multiple tau digital correlator with 288 exponentially spaced channels. The autocorrelation functions $[g^{(2)}(\tau) - 1]$ of the scattering curves were analyzed using the CONTIN program [15] developed by Provencher to give the distribution of the apparent diffusion coefficient, D_{app}. The apparent hydrodynamic radius, R_H, was then calculated using the Stokes–Einstein relationship, $R_H = kT/6\pi\eta D_{app}$, where k is the Boltz-

mann constant, T is the absolute temperature, and η is the viscosity of the solvent. Energy-filtered transmission electron microscopy (EF-TEM, Carl Zeiss EM912) was employed to observe the spherical vesicles.

3. Results and discussion

The steady-state fluorescence spectra for OBPV-21 as a function of concentration (1×10^{-7}–1×10^{-4} M) in *n*-hexane are shown in Figure 1B. Following the concentration gradient, the material exhibited drastic changes in the spectra. In the 1×10^{-6}–1×10^{-5} M transition, a new, redshifted, structured fluorescence spectrum centered at 480 nm abruptly intensified and contributed dominantly to the 1×10^{-4} M spectrum. This low-energy fluorescence spectrum was particularly well associated with vesicles that were tens of nanometer in size, as determined by dynamic light scattering (DLS) measurements and transmission electron microscopy (TEM) (inset of Figure 1B and in Figure 1C). In the inset of Figure 1B, a few micrometer sized particles deduced from the data was not reproducible, demonstrating that this minor component may originate from dust or similar.

The low-energy fluorescence spectrum was indicative of excimer formation in the *trans*-stilbene-like OBPV units, as depicted to the right in Figure 1C. When two *trans*-stilbene molecules are coupled, an excimer emission spectrum with several vibronic bands at lower energy is produced [16,17], similarly to that shown in Figure 1B. The self-assembly of triblock BA molecules containing a π-conjugated rod of sexithiophene [6] or oligo(*p*-phenylene vinylene) [7] and oligo(ethylene oxide) coils ($n = 4$ or 5) at each end exhibited excimer emissions under the molecular vesicle geometry sketched in the middle of Figure 1C. Note that vesicle formation and the subsequent excimer emission in OBPV-21 was successfully activated in apolar *n*-hexane by a plausible polar PPO coil-to-coil interaction, differently from earlier excimer emissions enabled via a hydrophobic interaction [6–8] in polar media. Further details of the polar coil-to-coil interaction will be discussed.

We obtained time-resolved fluorescence-decay profiles and steady-state excitation spectra as a function of concentration to further characterize the OBPV excimer emissions from the vesicles (Figure 2). Over the gradient from 1×10^{-6} to 1×10^{-5} M, the fluorescence time-decay profile probed at 480 nm abruptly became slower, while the excitation spectrum centered at 365 nm was blueshifted by 20 nm. These results were consistent with the abrupt fluorescence spectral changes shown in Figure 1B. The fluorescence time-decays were fitted to a sum of two exponential terms: an initial decay with a time constant 0.81 ± 0.02 ns and a subsequent decay characterized by a 5.0 ± 0.1 ns time constant. The faster decay with the time constant 0.81 ± 0.02 ns was dominant (97% in relative amplitude) for the molecularly dissolved states of 1×10^{-7}–1×10^{-6} M, while the slower decay with a 5.0 ± 0.1 ns time constant was dominant (95% in relative amplitude) for the vesicle states (1×10^{-5}–1×10^{-4} M). These time constants were principally attributed to the rates of relaxation from the excited-state OBPV monomer and the OBPV excimer, respectively.

As depicted at the right of Figure 1C, the coupling of two OBPV units resulted in H-type (cofacial rings) or J-type (stacked side-by-side) aggregates. The fluorescence lifetime of an H-aggregate is generally known to increase with respect to that of the monomer because of a disallowed transition to the ground state, whereas the J-aggregate has a reduced lifetime because of an allowed transition [18,19]. Another signature of the H-aggregate is a blueshifted excitation band due to dipole resonance coupling between the chromophores, which follows Kasha's rule [20,21]. Our two
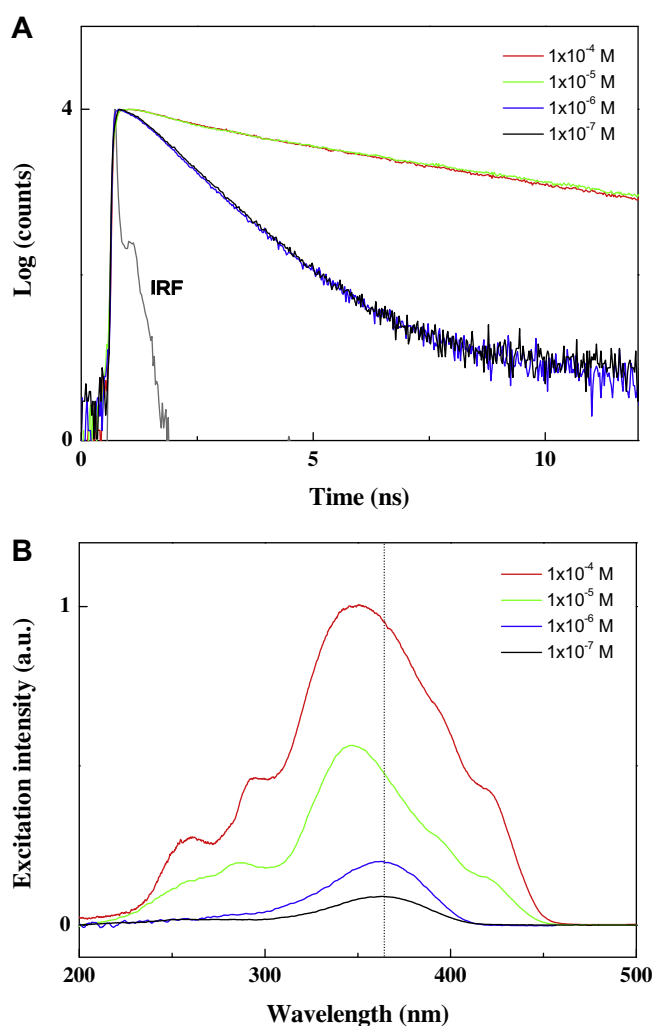
Figure 2. (A) Time-dependent fluorescence decay profiles of OBPV-21 as a function of concentration (1×10^{-7}–1×10^{-4} M) in *n*-hexane. The decays were measured at 480 nm. The excitation wavelength was 300 nm. 'IRF' indicates the instrument response function of the TCSPC system. (B) Excitation spectra for OBPV-21 as a function of concentration (1×10^{-7}–1×10^{-4} M) in *n*-hexane. The detection wavelength for the excitation spectra was 550 nm.

Figure 3. Fluorescence spectra for OBPV-13 (A) and OBPV-34 (B) as a function of concentration (1×10^{-7}–1×10^{-4} M) in *n*-hexane. The insets show the time-dependent fluorescence decay profiles measured for the 1×10^{-7} M (black) and 1×10^{-4} M (red) solutions at 480 nm. The excitation wavelengths for the steady-state and time-resolved data were 300 nm. (For interpretation of the references to colour in this figure legend, the reader is referred to the web version of this article.)

findings—the blueshifted excitation band and the slower decay (time-decay constant of 5.0 ± 0.1 ns)—suggested H-aggregation between the OBPVs in the vesicle state.

To investigate the effects of coil length on vesicle formation and the subsequent excimer emissions, we performed steady-state and time-resolved fluorescence studies for the OBPV-13 and OBPV-34 materials with shorter ($n = 13$) and longer ($n = 34$) PPO coils at the ends of the central OBPV units (Figure 3). At 1×10^{-4} M, OBPV-13 exhibited a monomer fluorescence spectrum centered at 420 nm, indicative of the predominant existence of the molecularly dissolved species. The structured vibronic bands of the excimer emission at 450–600 nm systematically grew sharper over the series OBPV-13 to OBPV-21 and OBPV-34, which was indicative of the more restricted vibrational or rotational motion of the OBPV in the more highly organized OBPV-34 vesicle (Figures 1B and 3A and B). The fluorescence decay time corresponding to the excimer emission increased from 3.0 ± 0.2 ns (OBPV-13) to 5.0 ± 0.1 ns (OBPV-21) and 5.7 ± 0.1 ns (OBPV-34), because of the retarded vibrational or rotational relaxations from the excited states of the more highly organized vesicles (Figure 2A, insets of Figure 3A
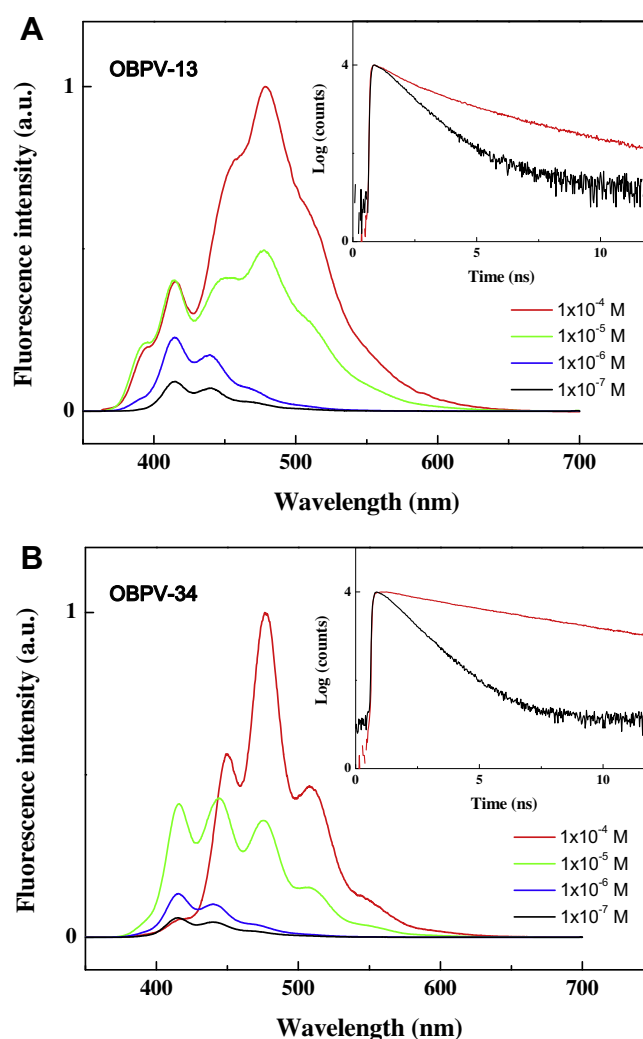
and B). Therefore, these findings indicate that, in apolar *n*-hexane solution, the strong polar coil-to-coil interaction between the longer PPO coils, rather than the hydrophobic rod-to-rod interaction, plays an important role in vesicle formation and the subsequent excimer emission.

Finally, we did not observe excimer emissions from a concentrated tetrahydrofuran (THF) solution of OBPV-21, despite nanoparticles that were hundreds of nanometer in size, as measured by DLS (Figure 4). The rods may be organized in such a way that the excimer emission is not possible. This finding indicated that, in the generation of the OBPV excimer, the hydrophobic interaction in polar THF was less effective than the polar coil-to-coil interaction in apolar *n*-hexane. An OBPV chromophore bound at both sides via strong polar coil-to-coil interactions may be more conducive to excimer formation, and thus, emission. We note that in other BA vesicle systems [6–8] most polar water was particularly employed as a solvent. When using water as a solvent, apolar interaction of the rod-rod and of the coil–coil cooperatively contributes to the vesicle formation. Contribution of this report may be to point out a process that generally occurs in BA vesicle systems.
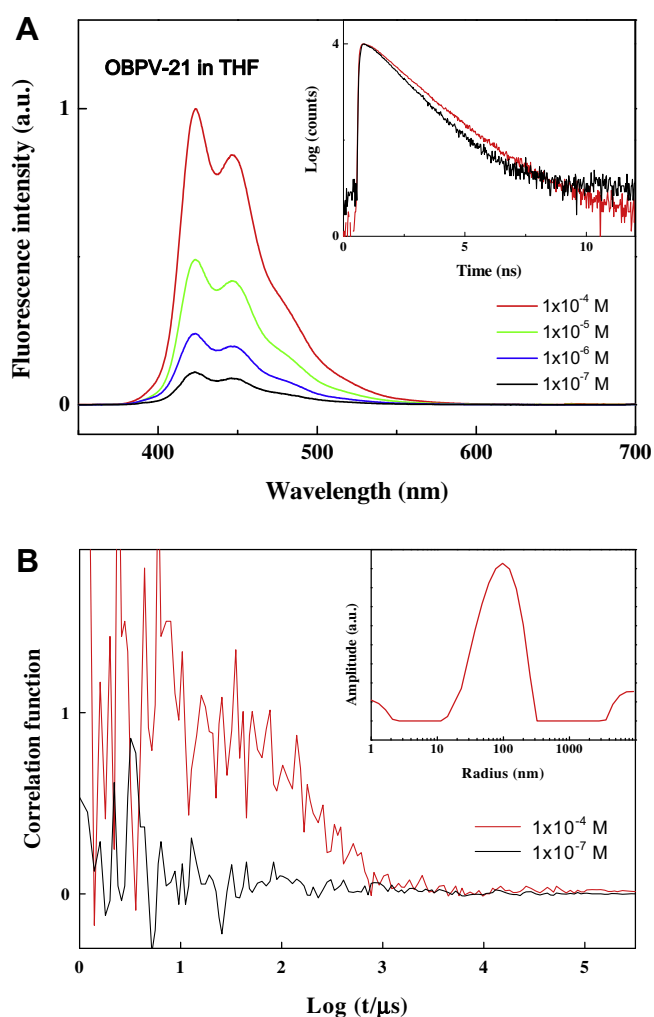
Figure 4. (A) Fluorescence spectra for OBPV-21 as a function of concentration (1×10^{-7}–1×10^{-4} M) in THF. The insets show the time-dependent fluorescence decay profiles measured for the 1×10^{-7} M (black) and 1×10^{-4} M (red) solutions at 480 nm. The excitation wavelengths for the steady-state and time-resolved data were 300 nm. (B) DLS autocorrelation traces for the 1×10^{-7} M (black) and 1×10^{-4} M (red) THF solutions of OBPV-21. The inset shows the size distribution function from the DLS data at 1×10^{-4} M. The first and third small peaks are artifacts from CONTIN analysis of the noisy data. (For interpretation of the references to colour in this figure legend, the reader is referred to the web version of this article.)

4. Conclusion

In summary, using a BA material comprising an OBPV hydrophobic rod with two polar coils of significantly long PPO ($n = 21$) at each end, a fluorescent vesicle was generated in concentrated n-hexane solution via a polar coil-to-coil interaction. The vesicle efficiently produced *trans*-stilbene-like OBPV excimer emissions, as evidenced by an intense, redshifted, structured fluorescence spectrum with a long fluorescence time-decay profile characterized by a time constant of 5.0 ± 0.1 ns. The longer fluorescence lifetime and the blueshifted excitation spectrum suggested H-aggregation between the OBPVs in the vesicle state. From analysis of the spectroscopic data obtained from OBPVs with different PPO coil lengths ($n = 13, 21, 34$), we found that the polar coil-to-coil interaction in apolar n-hexane, rather than a hydrophobic rod-to-rod interaction, played an important role in the generation of the OBPV excimer. This result was consistent with the absence of an excimer emission in the concentrated THF solution of OBPV-21, despite the presence of aggregated nanoparticles. An OBPV chromophore bound at both sides via a polar coil-to-coil interaction was more conducive to OBPV excimer formation and emission.

Acknowledgments

References

[1] J.-H. Fuhrhop, T. Wang, Chem. Rev. 104 (2004) 2901.
[2] I.-W. Hwang, Y.-R. Kim, Chem. Phys. Lett. 571 (2013) 34.
[3] X.L. Chen, S.A. Jenekhe, Langmuir 15 (1999) 8007.
[4] S.A. Jenekhe, X.L. Chen, Science 283 (1999) 372.
[5] A. Kaeser, A.P.H.J. Schenning, Adv. Mater. 22 (2010) 2985.
[6] I.O. Shklyarevskiy et al., J. Am. Chem. Soc. 127 (2005) 1112.
[7] F.J.M. Hoeben et al., Angew. Chem. Int. Ed. 45 (2006) 1232.
[8] X. Zhang, Z. Chen, F. Würthner, J. Am. Chem. Soc. 129 (2007) 4886.
[9] S.A. Jenekhe, X.L. Chen, Science 279 (1998) 1903.
[10] D.-H. Li et al., Macromol. Chem. Phys. 212 (2011) 297.
[11] M. Lee, J.-W. Kim, I.-W. Hwang, Y.-R. Kim, N.-K. Oh, W.-C. Zin, Adv. Mater. 13 (2001) 1363.
[12] I.E. Borissevitch, J. Lumin. 81 (1999) 219.
[13] I.-W. Hwang, N.W. Song, D. Kim, Y.T. Park, Y.-R. Kim, J. Polym. Sci., Part B: Polym. Phys. 37 (1999) 2901.
[14] D.V. O'Connor, D. Philips, Time-Correlated Single Photon Counting, Academic Press, New York, 1984.
[15] S.W. Provencher, Comp. Phys. 27 (1982) 229.
[16] M. Aguiar, B. Hu, F.E. Karasz, L. Akcelrud, Macromol. Chem. Phys. 199 (1998) 1255.
[17] M. Aguiar, L. Akcelrud, M.R. Pinto, T.D.Z. Atvars, F.E. Karasz, J. Saltiel, J. Photosci. 10 (2003) 149.
[18] N.C. Maiti, S. Mazumdar, N. Periasamy, J. Phys. Chem. B 102 (1998) 1528.
[19] N.C. Maiti, M. Ravikanth, S. Mazumdar, N. Periasamy, J. Phys. Chem. 99 (1995) 17192.
[20] M. Kasha, M.A. El-Bayoumi, W.J. Rhodes, J. Chim. Phys. 58 (1961) 916.
[21] R.M. Hochstrasser, M. Kasha, Photochem. Photobiol. 3 (1964) 317.